THE JOURNAL OF PHYSICAL CHEMISTRY B

Article

pubs.acs.org/JPCB

Effect of Unsaturation on the Absorption of Ethane and Ethylene in Imidazolium-Based Ionic Liquids

Leila Moura,[†,∥] Manas Mishra,[†] Varinia Bernales,[†,‡] Patricio Fuentealba,[§] Agilio A.H. Padua,[†] Catherine C. Santini,[∥] and Margarida F. Costa Gomes[†,*]

[†]Clermont Université, Université Blaise Pascal, Institut de Chimie de Clermont-Ferrand, UMR 6296 CNRS, équipe Thermodynamique et Interactions Moléculaires, ICCF-TIM, BP 80026, F-63171 Aubière, France

[‡]Departamento de Química, Facultad de Ciencias, Universidad de Chile, Las Palmeras #3425, Ñuñoa, Casilla 653-SCL, Santiago, Chile

[§]Departamento de Física, Facultad de Ciencias, Universidad de Chile, Las Palmeras #3425, Ñuñoa, Casilla 653-SCL, Santiago, Chile

[∥]Université de Lyon, Institut de Chimie de Lyon, UMR 5265 CNRS, Université de Lyon 1-ESCPE Lyon, LC2P2, Équipe Chimie Organométallique de Surface, 69616 Villeurbanne, France

Supporting Information

ABSTRACT: The influence of the presence of imidazolium side chain unsaturation on the solubility of ethane and ethylene was studied in three ionic liquids: 1-butyl-3-methylimidazolium bis(trifluoromethanesulfonyl)amide—saturated alkyl side-chain in the cation; 1-methyl-3-(buten-3-yl)imidazolium bis(trifluorosulfonyl)imide—double bond in the side-chain of the cation; and 1-methyl-3-benzylimidazolium bis(trifluorosulfonyl)imide—benzyl group in the side-chain of the cation. The solubility of both gases decreases when the side-chain of the cations is functionalized with an unsaturated group. This can be explained by a less favorable enthalpy of solvation. The difference of solubility between ethane and ethylene can be explained from a balance of enthalpic and entropic factors: for the ionic liquid with the saturated alkyl side-chain and the benzyl-substituted side-chain, it is the favorable entropy of solvation that explains the larger ethylene solubility, whereas in the case of the saturated side-chain, it is the more favorable enthalpy of solvation. Molecular simulation allowed the identification of the mechanisms of solvation and the preferential solvation sites for each gas in the different ionic liquids. Simulations have shown that the entropy of solvation is more favorable when the presence of the gas weakens the cation−anion interactions or when the gas can be solvated near different sites of the ionic liquid.

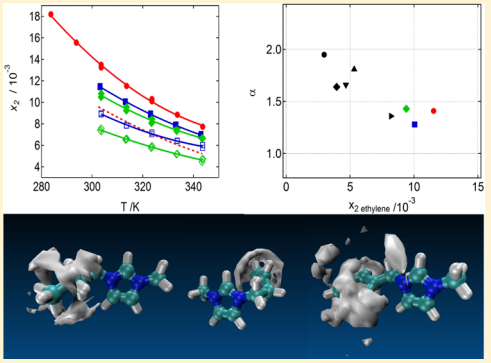

INTRODUCTION

Light olefins and paraffins are commonly separated by cryogenic distillation. Although reliable and still unchallenged in this application, this procedure implies high capital and operating costs. Thus the high demand for an alternative energy-saving separation process.[1−4]

Alternative processes for separating gaseous olefins from paraffins include ion exchanging resins,[5] adsorption on high-surface-area SiO_2,[6] on alumina,[7] on zeolites[8] and molecular sieves,[9] or on metallic organic frameworks,[10] and the use of several types of membranes.[3,11,12] Most of the alternatives proposed involve liquid or solid selective absorbents containing transition metals such as copper or silver, which are believed to form a complex with the unsaturated gas molecule.[1−3,13,14] These alternatives have not been applied to an industrial scale due to several drawbacks linked to the synthesis, the efficacy, the reliability or the contamination of the different materials and also related to economical obstacles.[1,2,15]

The molecular diversity of cations and anions that can form an ionic liquid and the general attractive properties of these fluids, including high thermal stability, negligible vapor pressure, and nonflammability, makes them good candidates as absorbents for gas separation.[16,17] Most of the published studies concerning the solubility of gases in ionic liquids involve the absorption of carbon dioxide, and much less report the solubility of light hydrocarbon gases in ionic liquids.[4] It has, nevertheless, been observed that unsaturated hydrocarbons, such as alkenes, are significantly more soluble in ionic liquids than their saturated counterpart[4,17] this fact being the basis for considering ionic liquids as possible absorbents to be used for hydrocarbon gas separation.[18,19]

The molecular mechanisms involved in the solvation of light hydrocarbon gases in ionic liquids are not yet well identified.[17] Several types of specific interactions between the unsaturated gases and the solvents have been suggested to explain their high solubilities such as $\pi-\pi$, π−cation, π−anion, and hydrogen

Received: March 28, 2013
Revised: May 27, 2013
Published: May 28, 2013

   dx.doi.org/10.1021/jp403074z | J. Phys. Chem. B 2013, 117, 7416−7425

bonding.[4,17,18,43] A deeper understanding of the solution's molecular structure and gas-solvent interactions is still necessary both for the design of an optimized ionic liquid and for the development of a potential separation process.

In the present study, we have designed a series of ionic liquids thought to favor the selective absorption of gaseous alkenes. We describe experimental solubilities of ethane and ethylene in these ionic liquids. Gas solubilities were measured as a function of temperature and at pressures close to atmospheric, using an isochoric saturation method. The knowledge of the variation with temperature of the solubility allows the calculation of the thermodynamic properties of solvation. Those can be related with molecular simulation calculations of the microscopic structure and molecular interactions in the gas-ionic liquid solutions in order to assess the mechanisms involved in the solvation of the different gaseous solutes.[20]

EXPERIMENTAL SECTION

Materials. Linde Gas supplied the gases used for this study: ethane 3.5, mole fraction purity of 0.9995 and ethylene 2.8, mole fraction purity of 0.998. All gases were used as received from the manufacturer.

1-Methylimidazole (>99%) (Aldrich), chlorobutane, benzyl chloride, 4-chloro-1-butene (>99%, Aldrich), and 3-chloro-1-propene (>99%, Aldrich) were distilled prior to use. Bis-(trifluoromethanesulfonyl)imide lithium salt (Solvionic) was used without further purification.

The ionic liquids used in this work, 1-butyl-3-methylimidazolium bis(trifluorosulfonyl)imide, $[C_1C_4Im][NTf_2]$, 1-methyl-3-(buten-3-yl)imidazolium bis(trifluorosulfonyl)imide, $[C_1(C_3H_5CH_2)Im][NTf_2]$, and 1-methyl-3-benzylimidazolium bis(trifluorosulfonyl)imide, $[C_1(CH_2C_6H_5)Im][NTf_2]$, were synthesized as previously reported and as described in the Supporting Information, SI.[21−23] Their structures are represented Figure 1.

The purity of the ionic liquid samples (>99%) was checked by ^1H and ^{13}C NMR (Bruker Avance 400 MHz using CD_2Cl_2 as solvent) and mass spectroscopy (see the SI). The high-resolution mass spectra (MS QTOF) were recorded in a positive and negative ion mode on a hybrid quadrupole time-of-flight mass spectrometer (MicroTOFQ-II, Bruker Daltonics, Bremen) with an Electrospray Ionization (ESI) ion source. The gas flow of spray gas is 6×10^{-4} Pa, and the capillary voltage is ±4.5 kV. The solutions are infused at 180 μL/h. The mass range of the analysis is 50−1000 m/z and the calibration was done with sodium formate.

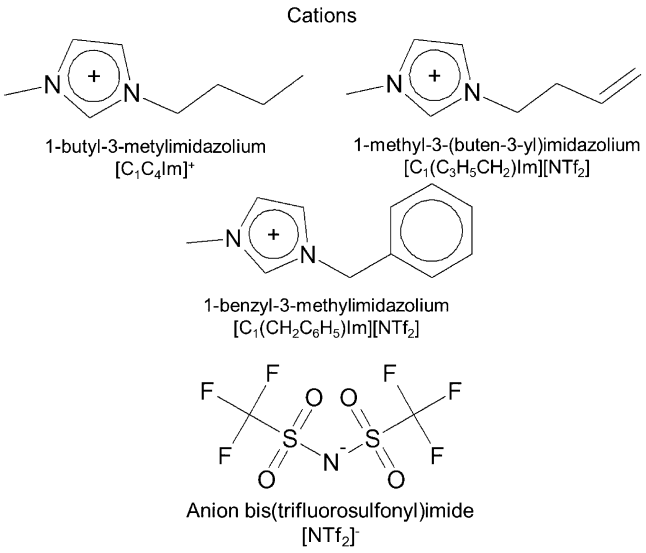

Figure 1. The structures and nomenclature system of the ionic liquids studied.

To remove water, the ionic liquid samples were kept under primary vacuum at least 24 h prior to use. Before each measurement, the water content of the degassed ionic liquid was verified with a coulometric Karl Fischer titrator (Mettler Toledo DL32). It was found to be lower than 100 ppm for $[C_1(C_3H_5CH_2)Im][NTf_2]$ and 70 ppm for $[C_1(CH_2C_6H_5)Im][NTf_2]$. The decomposition temperatures (T_{start}/T_{onset}) of the same ionic liquids were 482 K/579 and 564 K/599 K, respectively, determined using a DSC 2920 from TA Instruments.

Density Measurements. Density measurements were performed using a U-shaped vibrating-tube densimeter (Anton Paar, model DMA 512P) operating in a static mode. All measurements were performed at atmospheric pressure and at temperatures ranging from 283 to 353 K following a procedure described in previous publications.[24] The temperature was maintained constant within ±0.01 K by means of a recirculating bath equipped with a PID temperature controller (Julabo FP40-HP). The uncertainty of the density measurements is estimated as ±0.1 kg m^{-3}.

Viscosity Measurements. All of the viscosity measurements were performed with an Anton Paar AMVn rolling ball viscosimeter at atmospheric pressure and at temperatures between 293.15 and 373.15 K. The temperature was controlled to within 0.01 K and measured with accuracy better than 0.05 K. The measurements were performed using a 1.8 mm and a 3.0 mm diameter capillary tube that were calibrated as a function of temperature and angle of measurement using standard viscosity oils from Cannon (N35, S60, and N100). The overall uncertainty on the viscosity is estimated as ±1.5%.

Solubility Measurements. The solubility measurements were made using an isochoric saturation technique described in previous publications.[25−27]

In this technique, a known amount of gaseous solute is put in contact with a precisely determined amount of degassed ionic liquid, at constant temperature. At thermodynamic equilibrium, the pressure above the condensed phase is constant and directly related to the solubility of the gas in the fluid sample. The measurements were performed at temperatures between 303 and 343 K for $[C_1(C_3H_5CH_2)Im][NTf_2]$ and $[C_1(CH_2C_6H_5)Im][NTf_2]$ and between 283 and 343 K for $[C_1C_4Im][NTf_2]$.

The amount of ionic liquid sample is determined gravimetrically and the volume it occupies in the measuring cell, V_{liq}, is evaluated by the independent determination of the density at atmospheric pressure and as a function of temperature. This value is considered to be equal to the volume occupied by the solution after saturation with the gas. Since the ionic liquid does not present a measurable vapor pressure in the range of temperatures covered, the total amount of liquid is equal to its amount in the liquid solution, n_1^{liq} (subscripts 1 and 2 represent solvent and solute, respectively). The amount of solute in the liquid solution is obtained from the comparison between two pVT measurements: first when the gas is introduced in the cell and second when the thermodynamic equilibrium is attained:

dx.doi.org/10.1021/jp403074z | J. Phys. Chem. B 2013, 117, 7416−7425

$$n_2^{liq} = \frac{p_{ini} V_B}{[Z_2(p_{ini}, T_{ini})RT_{ini}]} - \frac{p_{eq}(V_{tot} - V_{liq})}{[Z_2(p_{eq}, T_{eq})RT_{eq}]} \quad (1)$$

where p_{ini} and T_{ini} are the pressure and temperature in the first pVT measurement and p_{eq} and V_{eq} correspond to the pressure and temperature after the system reaches the thermodynamic equilibrium, and V_B is the volume of the gas bulb. V_{tot} is the total volume of the equilibration cell, and Z_2 designates the compression factor for the pure gas.

The solubility results, expressed in mole fraction of the gas, are used to calculate the Henry's law constant, K_H:

$$K_H = \lim_{x_2 \to 0} \frac{f_2(p, T, x_2)}{x_2} \approx \frac{\phi_2(p_{eq}, T_{eq})p_{eq}}{x_2} \quad (2)$$

where f_2 is the fugacity of the solute, and ϕ_2 corresponds to the fugacity coefficient, calculated using the second virial coefficient of the gas.

Molecular Simulations. Ionic liquids were represented by an all-atom force field, which is based on the AMBER/OPLS–AA framework[28,29] with parameters developed specifically for the cations considered here.[30−32] For the $[C_1(C_3H_5CH_2)Im]$ cation, the force field parameters were determined in this work and are listed in the SI. The gases were modeled using OPLS-AA force fields.[28,33]

The ionic liquids were simulated in periodic cubic boxes containing 246 ion pairs, using the molecular dynamics method implemented in the DL_POLY package.[27] Initial low-density configurations, with ions placed at random in periodic cubic boxes, were equilibrated to attain liquid-like densities and structures at 373 K and 1 bar. Temperature and pressure were maintained using a Nosé-Hoover thermostat and barostat, respectively. Once the equilibrium density was attained, simulations runs of 400 ps were performed, with an explicit cutoff distance of 16 Å for nonbonded interactions, from which 5000 configurations were stored. Structural quantities such as radial and spatial distribution functions were calculated from configurations generated during the production runs. Additionally, simulation boxes containing 8 molecules of ethane and 8 molecules of ethylene separately were prepared in the same manner, to calculate solute−solvent radial distribution functions between the gas and the ionic liquid and the cation−anion interaction energy in the presence of the solute molecules.

The total energy of the simulated systems containing solute and ionic liquid was decomposed into contributions from different pairs of species, in order to quantify the predominant interactions. For that, the energy of each configuration (same atomic coordinates) was recalculated, taking into account only the relevant pairs of species, in turn. Also, the total energy was decomposed into intramolecular terms, short-range (Lennard–Jones) and electrostatic. In this manner, a detailed picture of the energetics of the system can be obtained.

RESULTS AND DISCUSSION

The experimentally measured densities of the ionic liquids $[C_1(C_3H_5CH_2)Im][NTf_2]$, and $[C_1(CH_2C_6H_5)Im][NTf_2]$ are reported in Table 1. Because the ionic liquids studied are relatively viscous, the experimental values of density were corrected, as recommended by the manufacturer, for the densimeter model used, by means of the equation:[34]

Table 1. Experimental Values for Densities, ρ, of the Studied Ionic Liquids, for Temperatures between 283 to 373 K and at Atmospheric Pressure, after Applying Correction factor, $\Delta\rho$

ρ (kg m^{-3})			
T (K)	$[C_1(C_3H_5CH_2)Im][NTf_2]$	T (K)	$[C_1(CH_2C_6H_5)Im][NTf_2]$
283.59	1482.5	282.80	1502.4
293.12	1472.8	293.15	1492.1
293.19	1463.1	302.75	1483.1
302.90	1472.8	302.82	1482.8
303.14	1463.2	313.13	1473.0
313.17	1453.6	321.87	1464.6
323.15	1444.1	333.06	1454.0
333.19	1434.6	342.81	1444.9
343.18	1425.3	352.90	1435.8
353.16	1416.2	363.03	1426.7
		372.82	1418.1

$$\frac{\Delta\rho}{\rho} = [-0.5 + 0.45\sqrt{n}]10^{-4} \quad (3)$$

The values found for $\Delta\rho$ vary between 0.09 kgm^{-3} at approximately 283 K to 0.009 kgm^{-3} at 373 K for $[C_1(CH_2C_6H_5)Im][NTf_2]$. The corrections are much lower to $[C_1(C_3H_5CH_2)Im][NTf_2]$, for which a maximum value of 0.03 kgm^{-3} was found for $\Delta\rho$ at 293 K.

The values of density were fitted to linear functions of temperature, the standard deviation of the fits being always better than 0.05%:

$$\rho_{[C_1(C_3H_5CH_2)Im][NTf_2]}/\text{kgm}^{-3} = 1751.7 - 0.95120 \times (T/K) \quad (4)$$

$$\rho_{[C_1(CH_2C_6H_5)Im][NTf_2]}/\text{kgm}^{-3} = 1766.9 - 0.93770 \times (T/K) \quad (5)$$

The densities of the two ionic liquids have been previously reported at 298 K by Mahurin et al.[35] (only for $[C_1(CH_2C_6H_5)Im][NTf_2]$) and by Mandai et al.[36] The value reported by Mahurin et al. has a lower precision than the ones reported herein and is significantly lower, a result compatible with the higher (and noncontrolled) amount of water of the ionic liquid used by the authors. The density values measured at 298 K by Mandai et al. agree with the ones measured here to within 0.1%.

The experimentally measured viscosities of the ionic liquids $[C_1(C_3H_5CH_2)Im][NTf_2]$ and $[C_1(CH_2C_6H_5)Im][NTf_2]$ are reported in Table 2. The experimental data were fitted as a function of temperature to a Vogel−Fulcher−Tammann (VFT) equation:

$$\eta = A \times T^{1/2} \exp\left(\frac{k}{T - T_0}\right) \quad (6)$$

the parameters of the fits are reported in Table 3.

It can be observed that $[C_1(CH_2C_6H_5)Im][NTf_2]$ is much more viscous than $[C_1(C_3H_5CH_2)Im][NTf_2]$, especially at the lower temperatures where the differences in viscosity are as high as 70% (or 137.4 mPa·s at 293 K). The difference in viscosity between the two liquids is much lower at the higher temperatures studied being of only of 40% at 353 K (or 6.27 mPa s).

dx.doi.org/10.1021/jp403074z | J. Phys. Chem. B 2013, 117, 7416−7425

Table 2. Experimental Values for the Viscosities the Studied Ionic Liquids, For Temperatures between 283 and 373 K

η (mPa·s)			
T (K)	$[C_1(C_3H_5CH_2)Im][NTf_2]$	T (K)	$[C_1(CH_2C_6H_5)Im][NTf_2]$
293.15	60.45	293.15	197.8
303.15	39.65	303.15	104.6
313.15	27.52	313.15	62.33
323.15	19.96	323.15	40.34
333.15	14.92	333.15	27.95
343.15	11.56	343.15	20.15
353.15	9.208	353.15	15.48
		363.15	12.05
		373.15	9.745

Table 3. Vogel–Fulcher–Tammann Equation Parameters Obtained for the Measurements of Viscosity, η, of $[C_1(C_3H_5CH_2)Im][NTf_2]$ and $[C_1(CH_2C_6H_5)Im][NTf_2]$ Ionic Liquids, For Temperatures between 283 and 373 K

η (mPa·s)				
	k (K)	$A/10^{-3}$ (mPa·s·K$^{-1/2}$)	T_0 (K)	AAD (%)
$[C_1(C_3H_5CH_2)Im][NTf_2]$	947	4.50	151	0.7
$[C_1(CH_2C_6H_5)Im][NTf_2]$	643	12.8	199	0.4

Orita et al.[37] have determined the viscosity of the ionic liquid $[C_1(C_3H_5CH_2)Im][NTf_2]$ at 298 K. Their value agrees with our measurements to within 3%. Mahurin et al.[34] and Mandai et al.[35] studied the viscosity of $[C_1(CH_2C_6H_5)Im][NTf_2]$ between 298 and 333 K and at 298 K, respectively. The present values are much higher than those reported in ref 34, the deviation of 57% being constant in the whole temperature range and compatible with the presence of a relatively large amount of water in the ionic liquid used. The value at 298 K reported in ref 35 is 13% lower than the one reported here, a difference more difficult to explain as the authors claim that their ionic liquid sample has a water content of less than 150 ppm, a value higher but sufficiently close to ours.

As depicted in Figure 2, the viscosity of $[C_1(C_3H_5CH_2)Im][NTf_2]$ is very similar to that of $[C_1C_4Im][NTf_2]$[38] (a difference of less than 3% in the whole temperature range), proving that the presence of a double bond on the side chain of the cation does not significantly affect the viscosity of imidazolium based ionic liquids. The same is not observed for $[C_1(CH_2C_6H_5)Im][NTf_2]$, even when its viscosity is compared with that of $[C_1C_8Im][NTf_2]$[39] (that has the same number of carbon atoms in the side-chain of the cation), for which a much higher viscosity was measured in the temperature range studied. We have also compared the viscosity of $[C_1(CH_2C_6H_5)Im][NTf_2]$ with that of 1-methyl-3-methylcyclohexylimidazolium bis(trifluorosulfonyl)imide, $[C_1(CH_2C_6H_{11})Im][NTf_2]$, reported by Mandai et al.[35] at 298 K. We have found that the viscosity of $[C_1(CH_2C_6H_{11})Im][NTf_2]$ is more than 100% higher than that of the ionic liquid containing the benzyl group in the side chain of the cation.

For each ionic liquid–gas pair, several solubility experimental data points were obtained for temperatures between 303 and 343 K in steps of approximately 10 K. The experimental solubilities obtained for ethane and ethylene in the ionic liquids $[C_1(C_3H_5CH_2)Im][NTf_2]$, and $[C_1(CH_2C_6H_5)Im][NTf_2]$ and

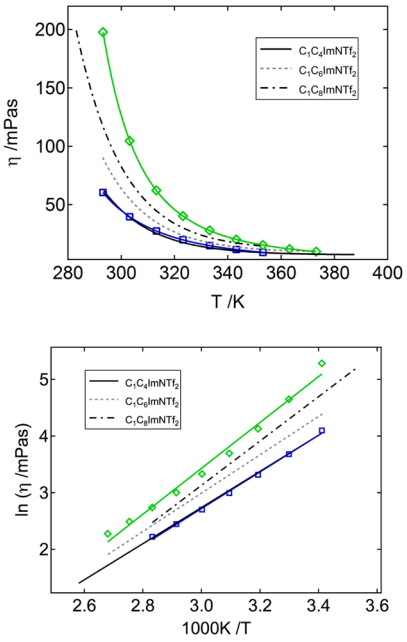

Figure 2. Viscosities of the studied ionic liquids: blue □, $[C_1(C_3H_5CH_2)Im][NTf_2]$, and green ◊, $[C_1(CH_2C_6H_5)Im][NTf_2]$ for temperatures between 283 and 373 K. Viscosity of $[C_1C_4Im][NTf_2]$,[38] $[C_1C_6Im][NTf_2]$,[45] and $[C_1C_8Im][NTf_2]$[39] added for comparison. The lines in the experimental data represent the VFT equation fitting using the parameters of Table 3.

for ethylene in $[C_1C_4Im][NTf_2]$ are reported in Table 4 and depicted in Figure 3, together with experimental results already published for ethane[26] in $[C_1C_4Im][NTf_2]$. For the calculation of the Henry's law constants, the compressibility factor, Z_2, and the fugacity coefficient, ϕ_2, were calculated from the second virial coefficient, obtained from the data compiled by Dymond and Smith.[40] The volume of ionic liquid in the equilibrium cell, V_{liq}, was obtained from the experimental density of the pure ionic liquid, as reported in Table 1.

The calculated Henry's law constants were fitted to a power series in T:

$$\ln[K_H/10^5\text{Pa}] = \sum_{i=0}^{n} A_i (T/K)^i \quad (7)$$

The coefficients A_i, being listed in Table 5. From the variation of the Henry's law constants with temperature, it is possible to calculate the thermodynamic properties of solvation as previously described.[26,41,42] The values obtained, at the temperature of 323 K, are listed in Table 6.

The solubility of ethylene in $[C_1C_4Im][NTf_2]$ has been previously measured by Anderson et al.[43] from 283 to 323 K. Our values of the Henry's law constant agree to within 0.6% at 323 K, the deviations increasing at lower temperatures to reach 13% at 283 K.

The solubility of the two studied gases is larger for $[C_1C_4Im][NTf_2]$ than for the two other liquids. This difference can be attributed to more negative enthalpies of solvation for both gases in $[C_1C_4Im][NTf_2]$.

For the three ionic liquids studied, ethylene is always more soluble than ethane in the temperature range covered. The higher solubility of ethylene can be explained, for $[C_1(C_3H_5CH_2)Im][NTf_2]$, by more favorable gas–ionic liquid interactions, as expressed by a more negative enthalpy of

dx.doi.org/10.1021/jp403074z | J. Phys. Chem. B 2013, 117, 7416–7425

Table 4. Experimental Values for the Solubility of Ethane, C_2H_6, and Ethylene, C_2H_4, in $[C_1(C_3H_5CH_2)Im][NTf_2]$ and $[C_1(CH_2C_6H_5)Im][NTf_2]$ Pure Ionic Liquids, and for ethylene, C_2H_4, in $[C_1C_4Im][NTf_2]$ Expressed Both As Henry'S Law Constants, K_H, and as Gas Mole Fraction, X_2, Corrected for a Partial Pressure of Solute of 0.1 MPa[a]

T(K)	p (10^2 Pa)	K_H (10^5 Pa)	X_2 (10^{-3})	%dev	T (K)	p(10^2 Pa)	K_H(10^5 Pa)	X_2(10^{-3})	%dev
C_2H_6 + $[C_1(C_3H_5CH_2)Im][NTf_2]$					C_2H_4 + $[C_1(C_3H_5CH_2)Im][NTf_2]$				
303.56	680.4	111.9	8.895	+ 0.7	303.12	639.2	87.30	11.42	− 0.4%
303.57	685.3	110.8	8.983	− 1.3	303.12	646.5	86.57	11.51	+ 0.0%
313.56	703.6	126.9	7.847	− 0.9	303.16	626.6	86.96	11.46	− 0.4%
313.58	708.7	127.2	7.829	− 1.1	313.09	648.4	99.47	10.02	− 0.3%
323.59	726.4	141.5	7.035	− 1.1	313.12	661.5	99.33	10.04	− 0.1%
323.60	731.5	138.6	7.184	+ 1.0	313.12	668.9	98.88	10.08	+ 0.4%
333.60	749.0	154.9	6.431	+ 0.1	323.00	670.0	112.8	8.841	− 0.1%
333.62	754.6	155.4	6.407	− 0.4	323.09	683.6	112.3	8.876	+ 0.4%
343.61	771.7	172.9	5.763	− 1.6	323.11	690.9	111.2	8.965	+ 1.4%
343.64	777.1	165.7	6.013	+ 2.7	332.91	691.3	126.2	7.902	+ 0.6%
303.56	680.4	111.9	8.895	+ 0.7	333.09	713.0	125.5	7.945	+ 1.4%
303.57	685.3	110.8	8.983	− 1.3	342.78	712.8	144.4	6.906	− 1.7%
313.57	703.6	126.9	7.847	− 0.9	342.94	727.3	144.3	6.911	− 1.4%
313.58	708.7	127.2	7.829	− 1.1	343.02	734.8	141.3	7.056	+ 0.7%
C_2H_6 + $[C_1(CH_2C_6H_5)Im][NTf_2]$					C_2H_4 + $[C_1(CH_2C_6H_5)Im][NTf_2]$				
303.25	656.7	134.4	7.408	− 1.2	303.55	675.0	94.91	10.50	− 1.6
303.55	881.6	135.9	7.315	− 1.9	303.58	680.7	92.09	10.82	+ 1.5
303.57	670.8	131.4	7.574	+ 1.5	313.53	698.2	107.9	9.241	− 1.5
313.29	679.6	152.5	6.530	− 0.8	313.60	704.3	104.2	9.560	+ 2.1
313.53	911.5	151.4	6.565	+ 0.2	323.49	721.3	123.4	8.079	− 2.8
313.57	693.8	150.1	6.633	+ 1.2	323.63	727.7	118.1	8.443	+ 1.7
323.35	702.4	172.8	5.762	− 1.0	333.42	743.9	136.0	7.331	− 1.2
323.56	716.7	169.6	5.871	+ 1.1	333.67	751.0	131.7	7.572	+ 2.3
323.61	941.6	167.7	5.931	+ 2.3	343.35	766.4	150.2	6.640	− 0.5
333.38	725.0	192.8	5.167	− 0.4	343.67	774.3	149.8	6.659	+ 0.1
333.56	739.4	190.8	5.220	+ 0.8					
343.38	747.9	223.7	4.454	− 4.4					
343.51	761.9	213.0	4.677	+ 0.5					
343.65	1002	209.8	4.744	+ 2.2					
C_2H_4 + $[C_1C_4Im][NTf_2]$									
283.67	803.0	54.62	18.19	+ 0.2					
293.76	833.8	63.91	15.56	+ 0.1					
303.57	872.4	75.11	13.24	− 1.3					
303.57	863.3	73.67	13.50	+ 0.6					
313.59	903.0	86.32	11.53	− 0.8					
323.61	923.2	96.64	10.30	+ 1.9					
323.61	933.3	98.55	10.10	− 0.1					
333.63	963.6	112.6	8.847	+ 0.0					
343.65	993.9	128.9	7.732	− 0.5					

[a] p is the experimental equilibrium pressure and the percent deviation is relative to the correlations of the data reported in Table 5.

solvation for C_2H_4 than for C_2H_6 (Table 6). For $[C_1(CH_2C_6H_5)Im][NTf_2]$ and $[C_1C_4Im][NTf_2]$, the higher solubility of ethylene is explained by more favorable entropies of solvation, an effect more pronounced in the case of $[C_1C_4Im][NTf_2]$ even if the difference in the ethane and ethylene solubility is larger for $[C_1(CH_2C_6H_5)Im][NTf_2]$ than for the two other ionic liquids.

Together with the amount of each gas that can be absorbed by the ionic liquid, the difference in solubilities is important for the design of gas separation processes and is normally quantified as the ideal selectivity of the separation, α, herein defined as follows:

$$\alpha = \frac{\frac{1}{K_H\text{ethylene}}}{\frac{1}{K_H\text{ethane}}} \quad (8)$$

This ideal gas selectivity is not very different from the real mixed gas selectivity as both gases present relatively low absorptions and so their activity coefficients in the liquid phase are close to unity.

In the upper plot of Figure 4, the selectivity is represented as a function of temperature for the ionic liquids studied (for ethane in $[C_1C_4Im][NTf_2]$ the data from Costa Gomes et al.[27] was used in the calculation). It is observed that the selectivity for $[C_1C_4Im][NTf_2]$ is similar to that for $[C_1(CH_2C_6H_5)Im][NTf_2]$ and constant over the temperature range covered. The selectivity for $[C_1(C_3H_5CH_2)Im][NTf_2]$ is slightly lower and decreases with increasing temperatures (as expected as the difference in solubilities is entropically controlled). In the lower plot of Figure 4, the performance plot is represented for ethylene (selectivity as a function of mole fraction solubility) of different ionic liquids. The larger selectivity was observed by

dx.doi.org/10.1021/jp403074z | J. Phys. Chem. B 2013, 117, 7416−7425

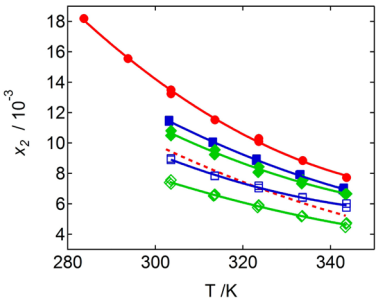

Figure 3. Mole fraction solubilities of ethane (empty symbols) and ethylene (full symbols) at 0.1 MPa partial pressure and as a functions of the temperature in the following ionic liquids: red ●, $[C_1C_4Im][NTf_2]$; blue ■/□, $[C_1(C_3H_5CH_2)Im][NTf_2]$; and green ♦/◇, $[C_1(CH_2C_6H_5)Im][NTf_2]$. Full lines represent the smoothed data using the parameters in Table 5 and the dashed line corresponds to the previously reported values of the solubility of ethane in $[C_1C_4Im][NTf_2]$.[27].

Table 5. Parameters of Eq 7 Used to Smooth the Experimental Results on K_H from Table 4 along with the Percent Average Absolute Deviation of the Fit, AAD

ionic liquid	A_0	A_1	A_2	% AAD
		C_2H_6		
$[C_1(C_3H_5CH_2)Im][NTf_2]$	− 4.782	49.77 × 10^{-3}	− 6.089 × 10^{-5}	0.9
$[C_1(CH_2C_6H_5)Im][NTf_2]$	+ 0.5989	16.20 × 10^{-3}	− 6.699 × 10^{-6}	1.4
		C_2H_4		
$[C_1(C_3H_5CH_2)Im][NTf_2]$	− 0.1297	17.55 × 10^{-3}	− 7.863 × 10^{-6}	0.5
$[C_1(CH_2C_6H_5)Im][NTf_2]$	− 2.750	34.80 × 10^{-3}	− 3.566 × 10^{-5}	1.5
$[C_1C_4Im][NTf_2]$	− 2.386	29.41 × 10^{-3}	− 2.428 × 10^{-5}	0.6

Table 6. Thermodynamic Properties of Solvation of Ethane and Ethylene, at 323 K, in $[C_1(C_3H_5CH_2)Im][NTf_2]$, $[C_1(CH_2C_6H_5)Im][NTf_2]$, and $[C_1C_4Im][NTf_2]$

ionic liquid	$\Delta_{solv}H^{\infty}$ (kJmol^{-1})	$T\Delta_{solv}S^{\infty}$ (kJmol^{-1}K^{-1})
	C_2H_6	
$[C_1(C_3H_5CH_2)Im][NTf_2]$	− 8.90 ± 0.1	− 22.2 ± 0.7
$[C_1(CH_2C_6H_5)Im][NTf_2]$	−10.1 ± 0.1	− 23.9 ± 0.7
$[C_1C_4Im][NTf_2]$[a]	−13.0 ± 0.1	− 26.3 ± 0.8
	C_2H_4	
$[C_1(C_3H_5CH_2)Im][NTf_2]$	− 11.1 ± 0.2	− 23.6 ± 0.7
$[C_1(CH_2C_6H_5)Im][NTf_2]$	− 9.52 ± 0.1	− 22.3 ± 0.5
$[C_1C_4Im][NTf_2]$	− 11.9 ± 0.1	− 24.2 ± 0.7

[a]Value from ref 27.

Camper et al.[44] for 1-ethyl-3-methylimidazolium dicyanamide, the larger ethylene absorption being reported herein for $[C_1C_4Im][NTf_2]$.

In order to get an insight on the molecular mechanisms responsible for the behaviors observed, we have analyzed the structure of the gas-ionic liquid solutions by calculating all the site−site solute−solvent radial distribution functions (RDFs) for all the solutions of gas in ionic liquid. As can be seen in Figure 5, where some of the most significant solute−solvent RDFs are plotted, the most striking differences on the structure of the solutions of the two gases are observed for the ionic liquid with the benzyl group in the cation (Figure 5c). In this

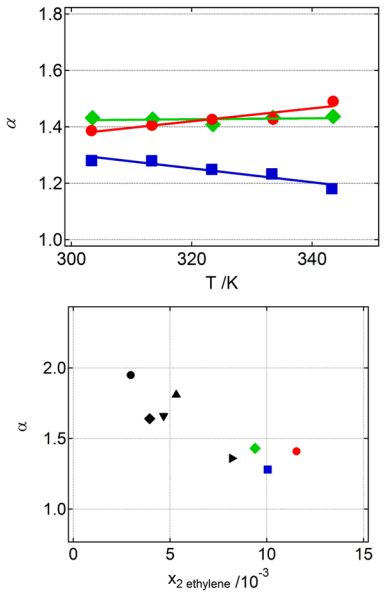

Figure 4. Upper plot: variation of the selectivity, α, as defined in eq 8 for the ethane/ethylene separation, with the temperature for the ionic liquids: red ●, $[C_1C_4Im][NTf_2]$; blue ■, $[C_1(C_3H_5CH_2)Im][NTf_2]$; green ♦, $[C_1(CH_2C_6H_5)Im][NTf_2]$. Lines represent the linear fitting of the data. Lower plot: variation of the selectivity as a function of the mole fraction solubility of ethylene, usually called performance plot, for ethylene at 313 K. ■ 1-hexyl-3-methylpyridinium bis-(trifluoromethylsulfonyl)imide ($[C_1C_6py][NTf_2]$;[43] ● 1-ethyl-3-methylimidazolium dicyanamide ($[C_1C_2Im][DCA]$);[44] ♦ 1-butyl-3-methylimidazolium tetrafluoroborate ($[C_1C_4Im][BF_4]$);[44] ▲ 1-butyl-3-methylimidazolium hexafluorophosphate ($[C_1C_4Im][PF_6]$);[44] ▶ 1-ethyl-3-methylimidazolium bis(trifluoromethylsulfonyl)imide ($[C_1C_2Im][NTf_2]$);[44] ▼ 1-ethyl-3-methylimidazolium trifluoromethanesulfonate ($[C_1C_2Im][CF_3SO_3]$).[44]

case, ethane has a larger probability of being found near the anion of the ionic liquid while ethylene interacts with a larger probability with the benzyl ring of the cation, an evidence of the preferential $\pi-\pi$ interaction between ethylene and the cation of the ionic liquid. A more detailed view is given by the spatial distribution functions represented in Figure 6, where it can be seen that ethane is preferentially solvated near the equatorial hydrogen atoms of the benzyl group and ethylene rests planar to the aromatic ring on the side chain of the cation. Also represented in Figure 6 is the probability of finding the gases solvated near the imidazolium ring of the cation—once again there is evidence that the ethylene molecule rests planar to the imidazolium ring, while ethane is solvated near the equatorial hydrogen atoms.

We have also decomposed the overall system configuration energy calculated by molecular simulation to the energy between each pair of species, as represented in Figure 7. The cation−anion interaction energy is more negative for $[C_1(CH_2C_6H_5)Im][NTf_2]$ in the presence of ethane than in presence of ethylene, an observation compatible with the higher entropy of solvation for ethylene that was observed experimentally. This difference on the total potential energy is due to a change on the electrostatic contribution, a fact that reinforces the conclusion that, in presence of ethane, the cation−anion interaction in the ionic liquid is stronger than in presence of ethylene.

Important differences can also be observed in Figure 5, parts a and b, for the two gaseous solutes in the other two ionic

dx.doi.org/10.1021/jp403074z | J. Phys. Chem. B 2013, 117, 7416−7425

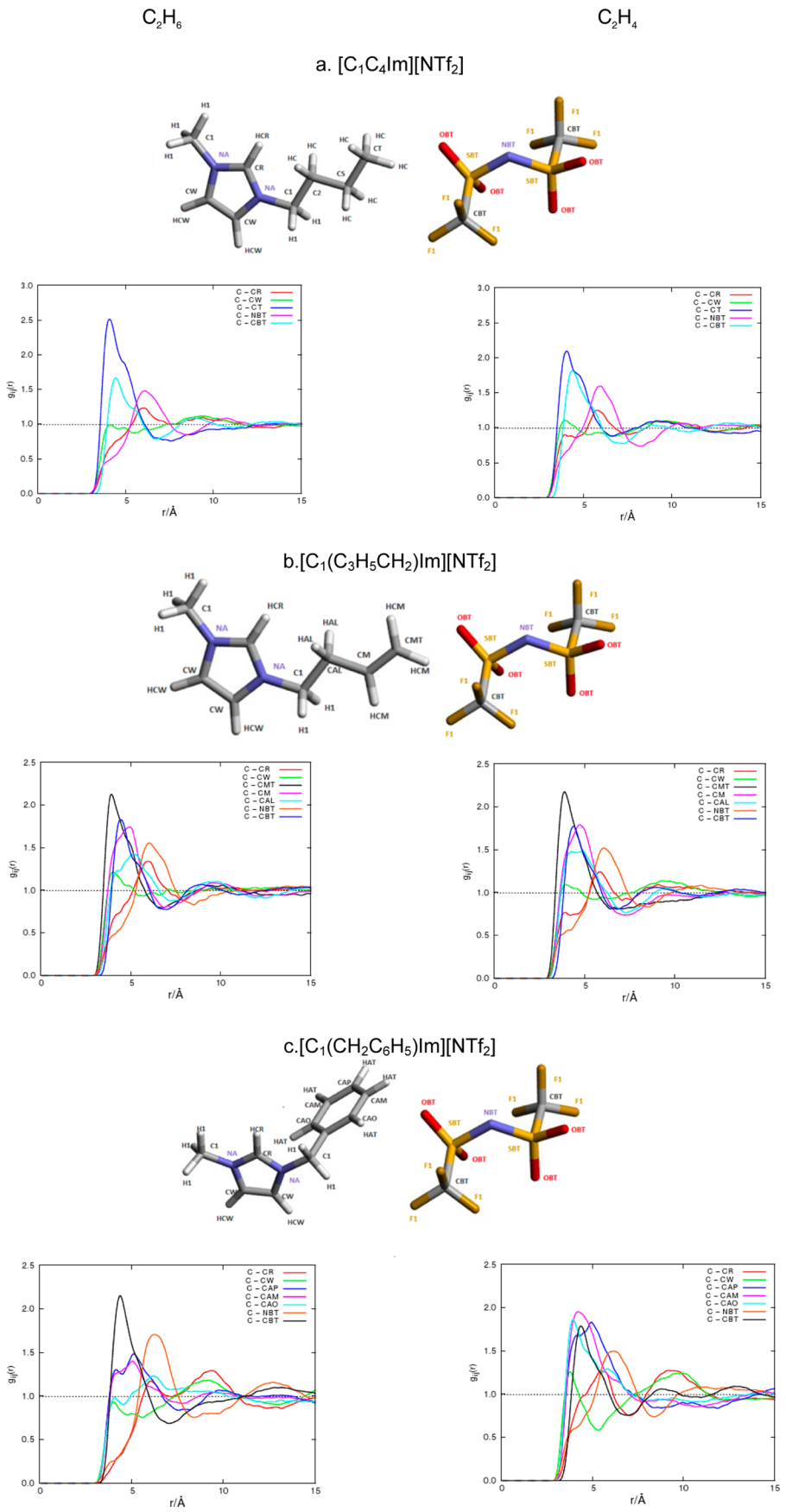

Figure 5. Site−site, solute−solvent radial distribution functions of ethane (plots on the left-hand side) and ethylene (plots on the right-hand side) for the three ionic liquids studied: $[C_1C_4Im][NTf_2]$ (first row); $[C_1(C_3H_5CH_2)Im][NTf_2]$ (second row) and $[C_1(CH_2C_6H_5)Im][NTf_2]$ (third row).

dx.doi.org/10.1021/jp403074z | J. Phys. Chem. B 2013, 117, 7416−7425

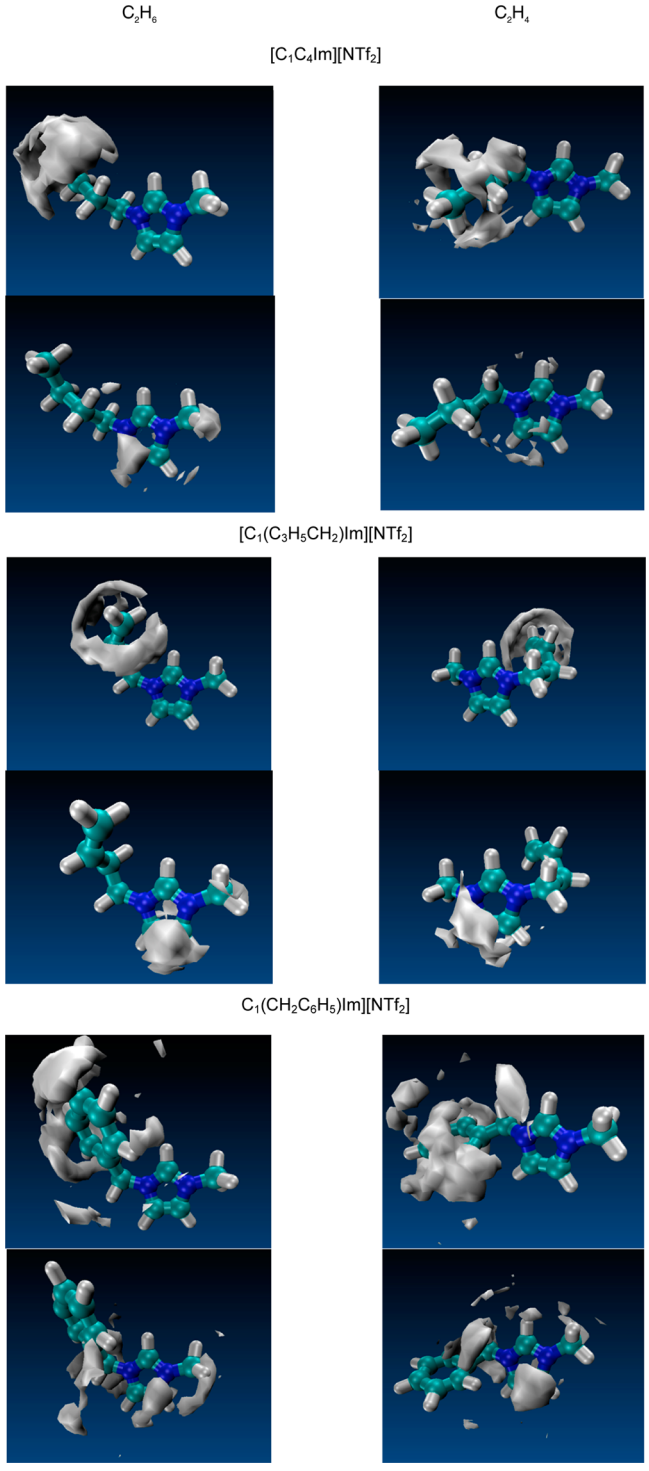

Figure 6. Spacial distribution functions of the center of mass of the two solutes around the terminal atoms of the alkyl-side chain of the cations or around the atoms of the imidazolium ring of the cation. The surface corresponds to an iso-probability density of 3.0 times the average density in the system.

liquids. For $[C_1C_4Im][NTf_2]$, both gases are solvated near the alkyl-side chain, but in the case of ethylene, the gas is preferentially solvated closer to the imidazolium ring. The interaction peak between the terminal atom of the alkyl-side chain and ethylene is wider than that with ethane, an observation indicating a larger mobility of the solute,

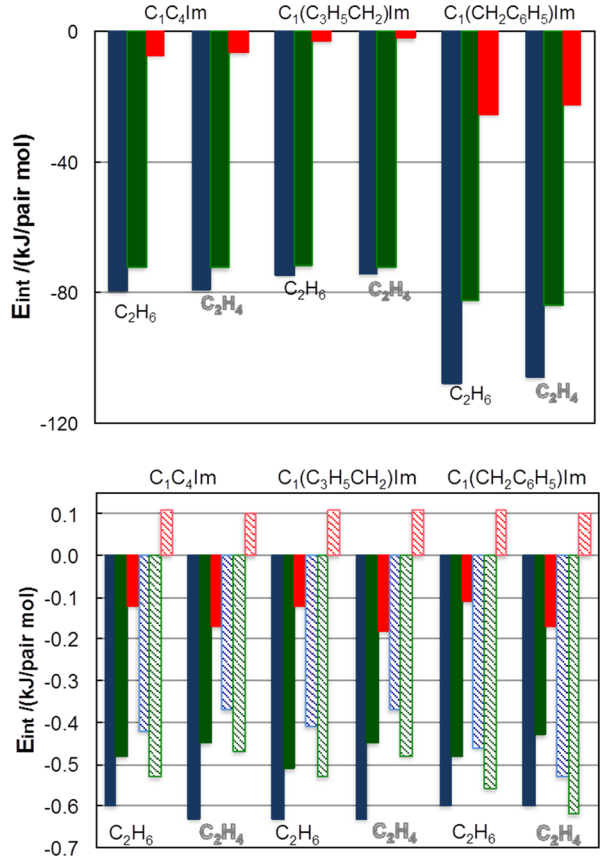

Figure 7. Energy decomposition calculated by molecular simulation. In blue, the total potential energy; in green, the dispersion interaction energy; and in red, the electrostatic contribution to the interaction energy. Upper plot: cation−anion interaction energy for the three ionic liquids in the presence of the two solutes. Lower plot: solute−ionic liquid interaction energies for the three ionic liquids. The filled bars represent the solute−anion interaction energy, and the patterned bars represent the solute−cation interaction energy.

compatible with the larger entropy of solvation found experimentally for this gas.

For the ionic liquid $[C_1(C_3H_5CH_2)Im][NTf_2]$, no significant differences are observed on the site−site solute−solvent radial distribution functions of the two gases (Figure 5b). In Figure 6, we can nevertheless observe a slight difference on the solvation of the two gases near the terminal atom of the alkyl side chain, with ethylene being more probably found on the extremity of the chain and ethane around the double bond.

■ CONCLUSIONS

From the study of the absorption of ethane and ethylene in different ionic liquids as a function of temperature, it was possible to determine the influence of the presence of unsaturated bonds on the cation on the solubility of the two gases. It was observed that the solubility of both ethane and ethylene decreases when the side-chain of the cation in the ionic liquid is functionalized with a double bond or a benzyl ring. This decrease of the solubility can be explained by a less favorable enthalpy of solvation.

The difference in solubility between ethane and ethylene is similar for the cation with the saturated alkyl side-chain and for the cation containing the benzyl ring but decreases for the cation with the double bond in the side chain. This behavior

dx.doi.org/10.1021/jp403074z | J. Phys. Chem. B 2013, 117, 7416−7425

results from a balance of enthalpic and entropic factors: for the two first ionic liquids ($[C_1C_4Im][NTf_2]$ and $[C_1(CH_2C_6H_5)Im][NTf_2]$), it is the favorable entropy of solvation that is responsible for the selectivity of the absorption of the two gases (ethylene always being the more soluble). For the ionic liquid containing a double bond on the side chain of the cation, $[C_1(C_3H_5CH_2)Im][NTf_2]$, it is the more favorable enthalpy that explains the larger ethylene solubility.

Computer simulations allow an interpretation at the molecular level of the observed solvation behaviors. Although the differences in solubility are similar, and attributed to favorable entropic contributions, for the ionic liquids $[C_1C_4Im][NTf_2]$ and $[C_1(CH_2C_6H_5)Im][NTf_2]$, the molecular reasons behind them are quite distinct. In the case of the ionic liquid with a benzyl substitution in the alkyl side-chain of the cation, the presence of ethylene decreases the cation−anion interaction, making the dissolution of C_2H_4 entropically more favorable. For the ionic liquid with the saturated alkyl side-chain, several solvation sites compete for the solvation of ethylene, probably contributing to a larger mobility of the solute and so a more positive entropy of solvation.

In the case of the ionic liquid with a double bond on the side chain of the cation, a more favorable interaction C_2H_4−$[C_1(C_3H_5CH_2)Im][NTf_2]$ explains the larger solubility of this gas.

■ ASSOCIATED CONTENT

Supporting Information

Details of the synthesis of the ionic liquids together with the NMR and the mass spectrometry analysis of the samples and the force field parameters for 1-methyl-3-(buten-3-yl)-imidazolium bis(trifluorosulfonyl)imide. This material is available free of charge via the Internet at http://pubs.acs.org.

■ AUTHOR INFORMATION

Corresponding Author

*E-mail: Margarida.c.gomes@univ-bpclermont.fr.

Notes

The authors declare no competing financial interest.

■ ACKNOWLEDGMENTS

The authors thank Dr. A. Podgorsek and Mr. F. Jacquet for the measurement of the viscosity of the ionic liquid $[C_1(C_3H_5CH_2)Im][NTf_2]$. L.M. is financed by a Cluster Excellence of the *Rhone Alpes* region, France with the participation of IFPEN, France. V.B. acknowledges CONICYT for the PhD fellowship and CONICYT-BECAS CHILE for supporting the research visit to Blaise Pascal University in France. Support by FONDECYT through Grant 11090013, Financiamiento Basal Para Centros Cientificos y Tecnologicos de Excelencia and also by Millennium Nucleus CILIS, Project ICM-P10-003-F is acknowledged.

■ REFERENCES

(1) Eldrige, R. B. Olefin/Paraffin Separation Technology: A Review. *Ind. Eng. Chem. Res.* **1993**, *32*, 2208−2212.

(2) Safarik, D. J.; Eldridge, R. B. Olefin/Paraffin Separations by Reactive Absorption: A Review. *Ind. Eng. Chem. Res.* **1998**, *37*, 2571−2581.

(3) Faiz, R.; Li, K. Olefin/Paraffin Separation Using Membrane Based Facilitated Transport/Chemical Absorption Techniques. *Chem. Eng. Sci.* **2012**, *73*, 261−284.

(4) Mokrushin, V.; Assenbaum, D.; Paape, N.; Gerhard, D.; Mokrushina, L.; Wasserscheid, P.; Arlt, W.; Kistenmacher, H.; Neuendorf, S.; Goeke, V. Ionic Liquids for Propene−Propane Separation. *Chem. Eng. Technol.* **2010**, *33*, 63−73.

(5) Sikavitsas, V. I.; Yang, R. T.; Burns, M. A.; Langenmayr, E. J. Magnetically Stabilized Fluidized Bed for Gas Separations: Olefin−Paraffin Separations by π-Complexation. *Ind. Eng. Chem. Res.* **1995**, *34*, 2873−2880.

(6) Dewitt, A.; Herwig, K.; Lombardo, S. Adsorption and Diffusion Behavior of Ethane and Ethylene in Sol-Gel Derived Microporous Silica. *Adsorption* **2005**, *11*, 491−499.

(7) Khan, A.; Riaz, M.; Butt, S. B.; Zaidi, J. H. Novel Modified Alumina: Synthesis, Characterization and Application for Separation of Hydrocarbons. *Sep. Purif. Technol.* **2007**, *55*, 396−399.

(8) van Miltenburg, A.; Zhu, W.; Kapteijn, F.; Moulijn, J. A. Adsorptive Separation of Light Olefin/Paraffin Mixtures. *Chem. Eng. Res. Des.* **2006**, *84*, 350−354.

(9) Xu, L.; Rungta, M.; Brayden, M. K.; Martinez, M. V.; Stears, B. A.; Barbay, G. A.; Koros, W. J. Olefins-Selective Asymmetric Carbon Molecular Sieve Hollow Fiber Membranes for Hybrid Membrane-Distillation Processes for Olefin/Paraffin Separations. *J. Membr. Sci.* **2012**, *423−424*, 314−323.

(10) Gucuyener, C.; van den Bergh, J.; Gascon, J.; Kapteijn, F. Ethane/Ethene Separation Turned on Its Head: Selective Ethane Adsorption on the Metal-Organic Framework ZIF-7 through a Gate-Opening Mechanism. *J. Am. Chem. Soc.* **2010**, *132*, 17704−17706.

(11) Ravanchi, M. T.; Kaghazchi, T.; Kargari, A. Application of Membrane Separation Processes in Petrochemical Industry: A Review. *Desalination* **2009**, *235*, 199−244.

(12) Kanezashi, M.; Kawano, M.; Yoshioka, T.; Tsuru, T. Organic−Inorganic Hybrid Silica Membranes with Controlled Silica Network Size for Propylene/Propane Separation. *Ind. Eng. Chem. Res.* **2011**, *51*, 944−953.

(13) Chen, L.; Liu, X. Q. π-Complexation Mesoporous Adsorbents Cu-MCM-48 for Ethylene−Ethane Separation. *Chinese J. Chem. Eng.* **2008**, *16*, 570−574.

(14) Kim, J.; Kang, S. W.; Mun, S. H.; Kang, Y. S. Facile Synthesis of Copper Nanoparticles by Ionic Liquids and Its Application to Facilitated Olefin Transport Membranes. *Ind. Eng. Chem. Res.* **2009**, *48*, 7437−7441.

(15) Azhin, M.; Kaghazchi, T.; Rahmani, M. A Review on Olefin/Paraffin Separation Using Reversible Chemical Complexation Technology. *J. Ind. Eng. Chem.* **2008**, *14*, 622−638.

(16) Costa Gomes, M. F.; Husson, P. Ionic Liquids: Promising Media for Gas Separations, Ionic Liquids: From Knowledge to Application; *ACS Symposium Series*; American Chemical Society: Washington DC, 2009, *1030*, 223−237.

(17) Gan, Q.; Zou, Y.; Rooney, D.; Nancarrow, P.; Thompson, J.; Liang, L.; Lewis, M. Theoretical and Experimental Correlations of Gas Dissolution, Diffusion, and Thermodynamic Properties in Determination of Gas Permeability and Selectivity in Supported Ionic Liquid Membranes. *Adv. Colloid Interfac.* **2011**, *164*, 45−55.

(18) Malik, M. A.; Hashima, M. A.; Nabi, F. Ionic Liquids in Supported Liquid Membrane Technology. *Chem. Eng. J.* **2011**, *171*, 242−254.

(19) Jung, S.; Palgunadi, J.; Kim, J. H.; Lee, H.; Ahn, B. S.; Cheong, M.; Kim, H. S. Highly Efficient Metal-Free Membranes for the Separation of Acetylene/Olefin Mixtures: Pyrrolidinium-Based Ionic Liquids as Acetylene Transport Carriers. *J. Membr. Sci.* **2010**, *354*, 63−67.

(20) Costa Gomes, M. F.; Padua, A. A. H. Gas−Liquid Interactions in Solution. *Pure Appl. Chem.* **2005**, *77*, 653−665.

(21) Campbell, P. S.; Santini, C. C.; Bouchu, D.; Fenet, B.; Philippot, K.; Chaudret, B.; Padua, A. A. H.; Chauvin, Y. A Novel Stabilisation Model for Ruthenium Nanoparticles in Imidazolium Ionic Liquids: In Situ Spectroscopic and Labelling Evidence. *Phys. Chem. Chem. Phys.* **2010**, *12*, 4217−4223.

(22) Gutel, T.; Santini, C. S.; Philippot, K.; Padua, A.; Pelzer, K.; Chaudret, B.; Chauvin, Y.; Basset, J. Organized 3D-Alkyl Imidazolium

Ionic Liquids Could be Used to Control the Size of in Situ Generated Ruthenium Nanoparticles? *J. Mat. Chem.* **2009**, *19*, 3624−3631.
(23) Stracke, M. P.; Ebeling, G.; Cataluna, R.; Dupont, J. Hydrogen-Storage Materials Based on Imidazolium Ionic Liquids. *Energy Fuels* **2007**, *21*, 1695−1698.
(24) Almantariotis, D.; Gefflaut, T.; Padua, A. A. H.; Coxam, J. Y.; Costa Gomes, M. F. Effect of Fluorination and Size of the Alkyl Side-Chain on the Solubility of Carbon Dioxide in 1-Alkyl-3-methylimidazolium Bis(trifluoromethylsulfonyl)amide Ionic Liquids. *J. Phys. Chem. B* **2010**, *114*, 3608−3617.
(25) Hong, G.; Jacquemin, J.; Deetlefs, M.; Hardacre, C.; Husson, P.; Costa Gomes, M. F. Correlations for Describing Gas-to-Ionic Liquid Partitioning at 323 K Based on Ion-Specific Equation Coefficient and Group Contribution Versions of the Abraham Model. *Fluid Phase Equilib.* **2007**, *257*, 27−34.
(26) Jacquemin, J.; Costa Gomes, M. F.; Husson, P.; Majer, V. Solubility of Carbon Dioxide, Ethane, Methane, Oxygen, Nitrogen, Hydrogen, Argon, and Carbon Monoxide in 1-Butyl-3-Methylimidazolium Tetrafluoroborate Between Temperatures 283 and 343 K and at Pressures Close to Atmospheric. *J. Chem. Thermodyn.* **2006**, *38*, 490−502.
(27) Costa Gomes, M. F.; Pison, L.; Pensado, A. S.; Padua, A. A. H. Using Ethane and Butane as Probes to the Molecular Structure of 1-Alkyl-3-Methylimidazolium Bis[(trifluoromethyl)sulfonyl]imide Ionic Liquids. *Faraday Discuss.* **2012**, *154*, 41−52.
(28) Smith, W. F.; Todorov, T. R. *The DL_POLY Molecular Simulation Package*, 2.20; STFC Daresbury Laboratories: Warrington, UK, 2007.
(29) Jorgensen, W. L.; Maxwell, D. S.; Tirado-Rives, J. Development and Testing of the OPLS All-Atom Force Field on Conformational Energetics and Properties of Organic Liquids. *J. Am. Chem. Soc.* **1996**, *118*, 11225−11236.
(30) (a) Chipot, C.; Jaffe, R.; Maigret, B.; Pearlman, D. A.; Kollman, P. A. Benzene Dimer: A Good Model for $\pi-\pi$ Interactions in Proteins? A Comparison Between the Benzene and the Toluene Dimers in the Gas Phase and in an Aqueous Solution. *J. Am. Chem. Soc.* **1996**, *118*, 11217−11224. (b) Udier-Blagović, M.; Morales De Tirado, P.; Pearlman, S. A.; Jorgensen, W. L. Accuracy of Free Energies of Hydration Using CM1 and CM3 Atomic Charges. *J. Comput. Chem.* **2004**, *25*, 1322−1332.
(31) Canongia Lopes, J. N.; Padua, A. A. H. *J. Phys. Chem. B* **2004**, *108*, 16893−16898.
(32) Canongia Lopes, J. N.; Deschamps, J.; Padua, A. A. H. Molecular Force Field for Ionic Liquids Composed of Triflate or Bistriflylimide Anions. *J. Phys. Chem. B* **2004**, *108*, 2038−2047.
(33) Kaminski, G.; Jorgensen, W. L. Performance of the AMBER94, MMFF94, and OPLS-AA Force Fields for Modeling Organic Liquids. *J. Phys. Chem.* **1996**, *100*, 18010−18013.
(34) Fandiño, O.; Pensado, A. S.; Lugo, L.; Comuñas, M. J. P.; Fernandez, J. Compressed Liquid Densities of Squalane and Pentaerythritol Tetra(2-ethylhexanoate). *J. Chem. Eng. Data* **2005**, *50*, 939−946.
(35) Mahurin, S. M.; Dai, T.; Yeary, J. S.; Luo, H.; Dai, S. Benzyl-Functionalized Room Temperature Ionic Liquids for CO_2/N_2 Separation. *Ind. Eng. Chem. Res.* **2011**, *50*, 14061−14069.
(36) Mandai, T.; Matsumura, A.; Imanari, M.; Nishikawa, K. Effects of Cyclic-Hydrocarbon Substituents and Linker Length on Physicochemical Properties and Reorientational Dynamics of Imidazolium-Based Ionic Liquids. *J. Phys. Chem. B* **2012**, *116*, 2090−2095.
(37) Orita, A.; Kamijima, K.; Yoshida, M. Allyl-Functionalized Ionic Liquids as Electrolytes for Electric Double-Layer Capacitors. *J. Power Sources* **2010**, *195*, 7471−7479.
(38) Jacquemin, J.; Husson, P.; Padua, A. A. H.; Majer, V. Density and Viscosity of Several Pure and Water-Saturated Ionic Liquids. *Green Chem.* **2006**, *8*, 172−180.
(39) Tokuda, H.; Tsuzuki, S.; Susan, A. B. H., Md.; Hayamizu, K.; Watanabe, M. How Ionic Are Room-Temperature Ionic Liquids? An Indicator of the Physicochemical Properties. *J. Phys. Chem. B* **2006**, *110*, 19593−19600.
(40) Dymond, J. H.; Marsh, K. N.; Wilhoit, R. C.; Wong, K. C. *The Virial Coefficients of Pure Gases and Mixtures, Landolt-Börnstein: Numerical Data and Functional Relationships in Science and Technology New Series, Subseries Physical Chemistry*; Springer: New York, 2003; 21B.
(41) Jacquemin, J.; Husson, P.; Majer, V.; Padua, A. A. H.; Costa Gomes, M. F. Thermophysical Properties, Low Pressure Solubilities and Thermodynamics of Solvation of Carbon Dioxide and Hydrogen in Two Ionic Liquids Based on the Alkylsulfate Anion. *Green Chem.* **2008**, *10*, 944−950.
(42) Almantariotis, D.; Fandino, O.; Coxam, J. Y.; Costa Gomes, M. F. Direct Measurement of the Heat of Solution and Solubility of Carbon Dioxide in 1-Hexyl-3-Methylimidazolium Bis-[trifluoromethylsulfonyl]amide and 1-Octyl-3-Methylimidazolium Bis-[trifluoromethylsulfonyl]amide. *Int. J. Greenhouse Gas Control* **2012**, *10*, 329−340.
(43) Anderson, J. L.; Dixon, J. K.; Brennecke, J. F. Solubility of CO_2, CH_4, C_2H_6, C_2H_4, O_2, and N_2 in 1-Hexyl-3-Methylpyridinium Bis(trifluoromethylsulfonyl)imide: Comparison to Other Ionic Liquids. *Acc. Chem. Res.* **2007**, *40*, 1208−1216.
(44) Camper, D.; Becker, C.; Koval, C.; Noble, R. Low Pressure Hydrocarbon Solubility in Room Temperature Ionic Liquids Containing Imidazolium Rings Interpreted Using Regular Solution Theory. *Ind. Eng. Chem. Res.* **2005**, *44*, 1928−1933.
(45) Chirico, R. D.; Diky, V.; Magee, J. W.; Frenkel, M.; Marsh, K. N. Thermodynamic and Thermophysical Properties of the Reference Ionic Liquid: 1-Hexyl-3-Methylimidazolium Bis-(trifluoromethylsulfonyl)imide (Including Mixtures). Part 2. Critical Evaluation and Recommended Property Values. *Pure Appl. Chem.* **2009**, *81*, 791−828.